

Short Communication

Preparation of Graphene Oxide Paper as an Electrode for Lithium-Ion Batteries Based on a Vacuum Filtration Method

Yi Lu^{1,2,3,*}, Tao Wang³, Zhaojun Tian³, Qing Ye³

¹ Hunan University of Science and Technology, Work Safety Key Lab on Prevention and Control of Gas and Roof Disasters for Southern Coal Mines, Xiangtan, Hunan 411201, China

² China University of Mining and Technology, School of Safety Engineering, Xuzhou, Jiangsu 221116, China

³ Hunan University of Science and Technology, School of Resource, Environment and Safety Engineering, Xiangtan, Hunan 411201, China

*E-mail: luyihust@163.com

Received: 2 June 2017 / Accepted: 13 August 2017 / Published: 12 September 2017

A conducting additive- and binder-free high-performance anode was prepared using freestanding graphene-graphene oxide paper (graphene/GO paper) for use in lithium-ion batteries (LIBs). The LIB anode comprised of graphene/GO paper exhibited a high rate performance and a high specific capacity of 702 mA h/g. This graphene/GO paper electrode fabricated by the facile assembly of graphene derivatives could be used to prepare flexible energy storage apparatuses.

Keywords: Lithium ion battery; Filtration method; Graphene paper; Graphene oxide; Energy storage

1. INTRODUCTION

Bendable or flexible electronic devices, including wearable apparatuses and roll-up displays, have garnered considerable interest in recent years. Additional requirements are necessary for the battery systems of these apparatuses, as the bendable property is mainly imparted by the flexibility of the electrode [1-3]. Traditional lithium-ion batteries (LIBs) possess electrodes that contain a mixture of a solvent, a binder, an electrical conductor, and an active material coated on a metal substrate [4, 5]. Due to the possibility of the substrate of the active material layer cracking or peeling off during repeated bending, this sort of electrode is not suitable for the preparation of bendable or flexible batteries. Therefore, the development of flexible, free-standing electrode materials for use in wearable and bendable batteries is highly desired. Previous studies by our group showed that single-walled carbon nanotubes (SWCNTs) may be used for the fabrication of free-standing electrodes for LIBs [6,

7]. The SWCNTs were regarded as an excellent substitute due to their one-dimensional structure and high length-to-diameter ratio. This sort of electrode is lightweight and highly flexible and is easily prepared without a binder or a metal substrate. Compared to traditional electrodes, the SWCNT free-standing electrode is less conductive, since it has no binder or substrate. Furthermore, due to the limitations of double-layer charge storage, the energy density of the CNT-containing electrodes was low, thus confining the charge and energy storage to only the active material surfaces [8]. The above disadvantages have greatly restricted their use in industry.

Graphene may be used in an extensive range of industrial applications, such as batteries/capacitors, electronic and structural components, thermal transport media, catalyst supports, adsorbents, or even biotechnological applications. Its excellent features, including mechanical hardness, electrical conductivity, thermal and chemical tolerance, as well as nontoxicity, make graphene well suited for these applications [9-14]. Composite structures consisting of graphene and CNTs were prepared by introducing SWCNTs into graphene planes via covalent C–C bonding, and may solve the above technical issues surrounding CNTs [15-18]. Wang and co-workers proposed the direct use of graphene film as a free-standing electrode for lithium-ion batteries [19]. Nevertheless, a capacity decrease to 100 mAh/g was observed after the first cycle at a current density of 50 mA/g, indicating poor cycling performance. This is primarily ascribed to the restacking of graphene layers during fabrication, suggesting that there is a close relationship between the arrangement of the layered structure in stacks of graphene sheets and their electrochemical behaviour.

In general, graphene suffers from two main weaknesses, despite its advantages in preparation and application. For graphene prepared from chemically decorated graphene derivatives (i.e., reduced graphene oxide (rGO), graphene oxide (GO), etc.), further thermal annealing is required for the complete recovery of the electrical features via the graphenization of the residual oxidized carbon atoms [20, 21]. Additionally, the interior structure of the as prepared GPs may be destroyed during the high-temperature annealing process, thus leading to fragile and brittle GPs, even under mild bending conditions. Furthermore, due to the dense restacking of the individual graphene layers during filtration, graphene prepared by vacuum filtration possesses a well ordered layer structure, resulting in the loss of some of the advantages of graphene in the film [20, 22]. In theory, compared to ordered graphene materials with a highly crystalline structure (i.e., graphitic carbon (372 mAh/g)), disordered graphene materials with a “house of cards” structure exhibit higher specific capacities of more than 780 mAh/g [23, 24]. Compared to traditional graphene electrodes, characterized by undesirable diffusion and intercalation of Li ions in the densely packed graphene layers, the polymer binder and graphene powder hybrids show improved electrochemical behaviour. Therefore, effective control of the graphene inter-sheet restacking is vital to ensure that the excellent inherent properties of the individual graphene sheets in graphene are maintained [25-27].

In this study, a wrinkle-structured graphene paper with high conductivity was prepared, in which GOs were incorporated into the paper as a film stabilizer and surfactant. Due to the presence of hydrophilic oxygen atoms in the functional groups on the basal planes and edges of the sheet, and the hydrophobic sp^2 graphene domains, the GO sheet is amphiphilic, and could be used as a two-dimensional surfactant in an aqueous system [28]. GO (a precursor of chemically derived graphene) could be used as an active Li storage material and a structural stabilizer due to its high specific

capacity, which allows for storage of as many Li ions as graphite [29]. The graphene/GO paper presented herein exhibited a relatively disordered and open structure with microscopic wrinkles, which is ascribed to partial graphene aggregation under the holding and stabilizing effects of the GO during the drying process. Based on the above structural properties, the new graphene/GO paper was used as a highly flexible LIB anode with remarkable electrochemical behaviour. Additionally, this graphene/GO paper has potential applications in the fabrication of foldable and flexible energy storage apparatuses.

2. EXPERIMENTAL

2.1. Synthesis of GO and graphene dispersions

A modified Hummer's route was used for the synthesis of GO. The final GO powder was dispersed in deionized (DI) water and bath-sonicated for 20 min, followed by centrifugation at 6000 rpm to remove any multi-layer species. The supernatant was used for the preparation of a 0.5 mg/mL GO dispersion in a stable state. A small volume of poly(4-styrenesulfonic acid) (PSS) solution was introduced into a 0.5 mg/mL dispersion of the graphene nanoplatelet powder in DI water to facilitate the initial wetting between water and graphene. The dispersion was then stabilized with a horn sonicator for 3 h. The graphene/GO paper was prepared as follows: GO solutions were mixed with the dispersed graphene at a volume ratio of 3:1 for graphene:GO, then an equal volume of DI water was introduced, followed by bath sonication for 10 min to promote dispersion.

2.2. Preparation of the graphene/GO paper

The graphene/GO mixture was filtered under vacuum through a polyvinylidene fluoride (PVDF) filter and then air-dried. Separation from the filter membrane yielded graphene/GO papers. The *ca.* 5 μm thick graphene/GO papers prepared from the graphene/GO mixture (20 mL) were used throughout this work, unless otherwise stated. For the thermally annealed samples, the graphene/GO paper was treated at 350 °C in air for 60 min, after which, the remaining PSS polymer surfactant and oxygen-containing functional groups present on the GOs were removed.

2.3. Measurements

A JANDEL RM3 four-point probe was used to measure the conductivity. The test electrodes were prepared using the free-standing films, based on CR 2032 coin-type cells assembled in an Ar-filled glove box (Mbraun, Unilab, Germany). The anodes were stacked using a reference electrode, a lithium foil counter electrode, and a porous polypropylene separator. Dimethyl carbonate was mixed with ethylene carbonate in a 50:50 (v/v) ratio, and then added to LiPF_6 (1 M) to yield the test electrolyte. A Cu $K\alpha$ ($\lambda = 1.5418 \text{ \AA}$) source was applied to a Rigaku Rotaflex RU-200B diffractometer equipped with a Ni filter, and used for the crystallographic investigation at 40 kV and 40 mA with a scan rate of 0.02 s^{-1} . A J.A. Woollam variable angle spectroscopic ellipsometer (J.A. Woollam Co.,

Lincoln, NE) was used for measuring the thickness at an incidence angle of 70° and a wavelength range of 380–1000 nm using the AutoRetarder feature for high polarization measurement accuracy. For the galvanostatical charge and discharge of the cells, the temperature and current density were 20°C and 30 mA/g, respectively, and the voltage window ranged from 0.01 to 3.0 V (vs. Li/Li⁺). The discharge capacities were based on the total amount of free-standing electrode. CV was performed at a scan rate of 100 mV/s in the potential range of 0.0–3.0 V. Electrochemical impedance spectroscopy (EIS) measurements were carried out using an Ametek PARSTAT 2273 electrochemistry workstation, with an AC amplitude of 5 mV and a frequency range of 100 kHz–0.01 Hz.

3. RESULTS AND DISCUSSION

Fig. 1 displays the X-ray diffraction (XRD) profiles of the microstructure of the new graphene/GO paper along with the analysis of the stabilization effect of the GOs. A single peak centred at $2\theta = 11.6^\circ$ was observed for the paper prepared from only GOs, consistent with the interlayer distance (d -spacing) of ca. 0.725 nm, indicating that the individual GO sheets stacked in a highly ordered manner during the flow-directed assembly [30]. Compared to traditional graphene, the graphene/GO paper showed multiple XRD profiles, due to the varying surface structures and morphologies in its two components. The interlayer spacing between individual graphene sheets showed a peak centred at $2\theta = 25.2^\circ$, which is consistent with what was observed in general GPs after they had undergone a thermal reduction process [31]. Due to the spacing between graphene and GO, a unique peak, which is not present in general graphene, centred at $2\theta = 16.6^\circ$ was observed; this peak suggests that the GO sheets are uniformly dispersed between the graphene layers in the graphene/GO papers. Despite the thorough separation of the majority of the single-layer GO sheets through centrifugation, several multi-layered GO sheets may also be present in the GO dispersion, leading to a low intensity peak near $2\theta = 11.8^\circ$, consistent with the presence of stacked GOs. This observation confirmed that the majority of the GOs had inserted between the graphene sheets in the final graphene/GO paper. Through the incorporation of GO sheets, the spacing between the stacked graphene layers had increased, allowing for the full use of the effective surface area, and increasing the storage sites for Li ions [32]. Furthermore, the graphene/GO paper exhibited another peak centred at $2\theta = 26.5^\circ$, which can be attributed to the folded and wrinkled graphene sheet structures [33]. For the hydrated graphene, extrinsic wrinkles were formed, resulting in locally corrugated and folded structures imparted by the tensile stress incurred during the drying process. The above structural phenomena, such as the expanded spacing and folded structure of the graphene layers, found in the graphene/GO paper could lead to an enhancement in the Li storage capacity when used as an LIB electrode.

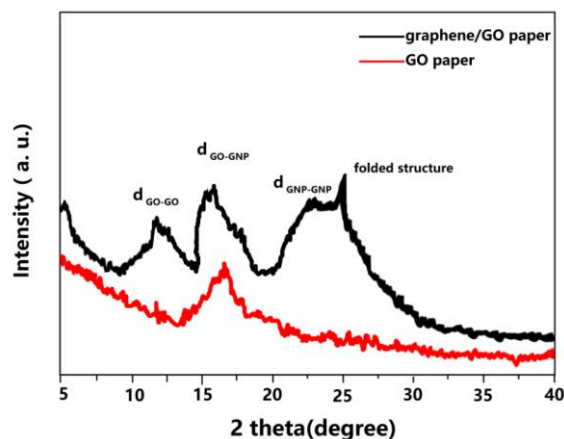


Figure 1. XRD profiles of the graphene/GO paper and a GO paper.

The graphene/GO paper was highly electrically conductive, and possessed excellent structural properties. Furthermore, the graphene/GO paper required no additional treatment, which was necessary due to the materials used to fabricate the electrode. As shown in Fig. 2, the electrical conductivity of the graphene/GO paper varied with the thickness of the paper. When the paper thickness was 15 μm , the maximum conductivity was obtained at approximately 176 S/cm. This result varied only slightly after the graphene/GO paper had undergone the annealing treatment, indicating that the insulating effect of the nonconductive GOs could be neglected. The paper-like structure and relatively high electrical conductivity of the GNP/GO paper enabled its direct utilization as an electrode, without requiring a conducting additive, binder or a metal current collector, which can lead to the enhancement of the energy density of a device [34, 35].

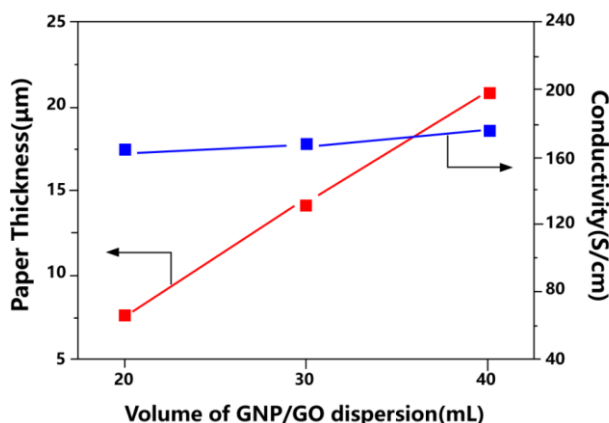


Figure 2. Variation in the graphene/GO paper thickness vs. graphene/GO dispersion volume for a vacuum filtration. A slight increase in the graphene/GO paper conductivity was observed with the increased paper thickness. The blue squares represent the paper conductivity measured using a thermally annealed (10 min, 350 °C, in air) graphene/GO dispersion (40 mL). The red squares represent the paper conductivity measured using a graphene/GO dispersion (2/1 ratio by weight).

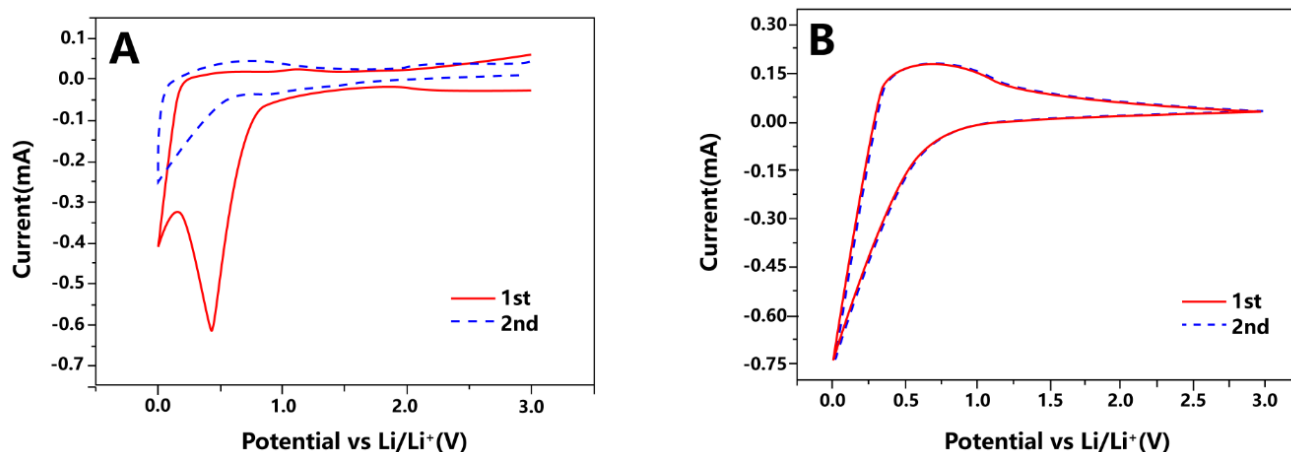


Figure 3. (A) CV profiles of the graphene/GO paper anode for the first two cycles. Scan rate: 0.1 mV/s. (B) CVs for the graphene/GO paper after thermal annealing for 60 min at 350 °C in air.

The binder- and conducting additive- free anode for LIBs was successfully prepared using graphene/GO paper, and its electrochemical behaviour was explored. A reductive peak (1.0 - 0.24 V) was observed in the cyclic voltammetry (CV) profile of the graphene/GO paper anode but only in the initial cycle (Fig. 3A). The solid-electrolyte interphase (SEI) film arises from the reaction between active lithium metal and the components of the electrolyte solution, including organic solvents and anions of lithium salt [36, 37]. This result is consistent with that of the CV profile for the graphene/GO paper anode after thermal annealing, in which no distinguishable peak was observed apart from the Li insertion peak at 1.0 V, as shown in Fig. 3B.

The four initial charge/discharge cycles were characterized via the voltage patterns at a constant current density of 50 mA/g, as shown in Fig. 4A. Only the first discharge pattern displayed a potential plateau at ca. 1.0 V. This result was evident in the CVs. The maximum value for the initial discharge capacity was 2900 mA h/g, with an irreversible 78% loss, possibly due to the electrochemical reduction of the GO, forming an SEI layer. In the following cycles, a decrease in the irreversible capacity loss was observed for the graphene/GO paper anode, which exhibited a high irreversibility for the initial cycle. This suggests that the properties of the SEI film dramatically change (such as when the film is broken) during cycling, which gives rise to a higher resistance for the transfer of Li-ions. This change indicates that the film is repeatedly broken during cycling. However, the broken SEI film can be repaired by the reaction between the lithium electrode and the components of the electrolyte solution [38]. This phenomenon suggested that potential side reactions (i.e., the reduction of GO) occurred mainly during the initial cycle and were completed after several cycles.

Fig. 4B shows the cycle behaviour of the graphene/GO paper anode (current density: 50 mA/g). The initial charge capacity was a low value of 702 mA h/g (coulombic efficiency, 27%), which then quickly increased to greater than 90% after several cycles. After 55 cycles, the charge capacity was maintained at 530 mA h/g (capacity retention, 73.1%). In general, the well-ordered structure of the graphene anode functioned as a kinetic barrier for the diffusion of Li ions from the anode during the lithiation process.

The rate performance of the graphene/GO paper anode was investigated at current densities of 100, 200, 300, 500, 1000, and 2000 mA/g, with the reversible specific capacities of 527, 414, 325, 271, 198, and 146 mA h/g, respectively, as shown in Fig. 4C. The reversible capacity returned to 592 mA h/g with a current density of 50 mA/g, suggesting that the graphene/GO paper anode possessed a high rate capability. The graphene/GO paper anode had highly stable electrochemical behaviour and specific capacity due to the assistance of the GO sheets (characteristic of folded and wrinkled structure) in the formation of a porous graphene stacking, which further facilitated the diffusion and storage of Li ions.

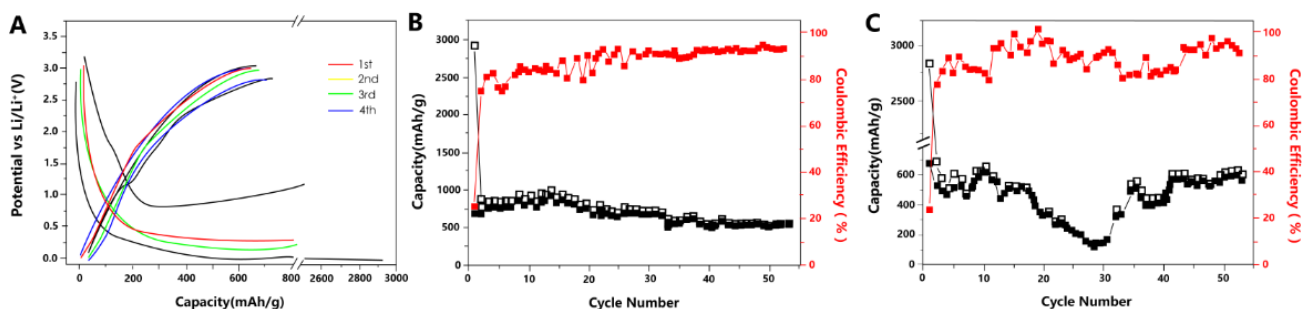


Figure 4. (A) Galvanostatic discharge/charge potential patterns of the initial four cycles. Current density: 50 mA/g. (B) Specific capacity and coulombic efficiency vs. the serial number of cycles. Current density: 50 mA/g. (C) Specific capacity and coulombic efficiency vs. the serial number of cycles at varying current densities of 100, 200, 300, 500, 1000, and 2000 mA g⁻¹ after the first cycle at 50 mA/g.

4. CONCLUSIONS

In this work, a time-saving filtration route was used for the synthesis of multi-layer graphene sheets. GOs were used as active Li storage materials and film stabilizers, and neither binders nor conducting additives were required. The free-standing graphene/GO paper showed superior charge capacity and low charge transfer resistance. Due to the average *d*-spacing enlargement, the ionic conductivity enhancement imparted by the distinct sandwich structure with efficient conductive paths, and the promotion of the electrode electronic conductivity imparted by the decrease in electrode thickness and increase in mass density, Li cycling behaviour was improved, thus leading to more sites to accommodate the Li ions.

ACKNOWLEDGEMENT

This work was supported by the National Natural Science Foundation of China (51604110), Provincial Natural Science of Hunan (2017JJ3074).

References

1. H. Gwon, H. Kim, K. Lee, D. Seo, Y. Park, Y. Lee, B. Ahn and K. Kang, *Energy & Environmental Science*, 4 (2011) 1277.
2. L. Hu, F. La Mantia, H. Wu, X. Xie, J. McDonough, M. Pasta and Y. Cui, *Advanced Energy Materials*, 1 (2011) 1012.
3. G. Xu, C. Zheng, Q. Zhang, J. Huang, M. Zhao, J. Nie, X. Wang and F. Wei, *Nano Research*, 4 (2011) 870.
4. J. Tarascon and M. Armand, *Nature*, 414 (2001) 359.
5. A. Aricò, P. Bruce, B. Scrosati, J. Tarascon and W. Van Schalkwijk, *Nature Materials*, 4 (2005) 366.
6. S. Ng, J. Wang, Z. Guo, J. Chen, G. Wang and H. Liu, *Electrochimica Acta*, 51 (2005) 23.
7. S. Chew, S. Ng, J. Wang, P. Novák, F. Krumeich, S. Chou, J. Chen and H. Liu, *Carbon*, 47 (2009) 2976.
8. H. Byon, B. Gallant, S. Lee and Y. Shao-Horn, *Adv Funct Mater*, 23 (2013) 1037.
9. S. Stankovich, D. Dikin, G. Dommett, K. Kohlhaas, E. Zimney, E. Stach, R. Piner, S. Nguyen and R. Ruoff, *Nature*, 442 (2006) 282.
10. S. Guo, S. Dong and E. Wang, *ACS Nano*, 4 (2009) 547.
11. A. Balandin, S. Ghosh, W. Bao, I. Calizo, D. Teweldebrhan, F. Miao and C. Lau, *Nano Letters*, 8 (2008) 902.
12. F. Schedin, A. Geim, S. Morozov, E. Hill, P. Blake, M. Katsnelson and K. Novoselov, *Nature Materials*, 6 (2007) 652.
13. S. Gilje, S. Han, M. Wang, K. Wang and R. Kaner, *Nano Letters*, 7 (2007) 3394.
14. Z. Liu, J. Robinson, X. Sun and H. Dai, *Journal of the American Chemical Society*, 130 (2008) 10876.
15. M. Zhao, X. Liu, Q. Zhang, G. Tian, J. Huang, W. Zhu and F. Wei, *ACS Nano*, 6 (2012) 10759.
16. Q. Zheng, B. Zhang, X. Lin, X. Shen, N. Yousefi, Z. Huang, Z. Li and J. Kim, *Journal of Materials Chemistry*, 22 (2012) 25072.
17. Y. Wu, T. Zhang, F. Zhang, Y. Wang, Y. Ma, Y. Huang, Y. Liu and Y. Chen, *Nano Energy*, 1 (2012) 820.
18. M. Zhao, Q. Zhang, J. Huang, G. Tian, T. Chen, W. Qian and F. Wei, *Carbon*, 54 (2013) 403.
19. C. Wang, D. Li, C. Too and G. Wallace, *Chemistry of Materials*, 21 (2009) 2604.
20. H. Chen, M.B. Müller, K. Gilmore, G. Wallace and D. Li, *Adv. Mater.*, 20 (2008) 3557.
21. C. Chen, J. Huang, Q. Zhang, W. Gong, Q. Yang, M. Wang and Y. Yang, *Carbon*, 50 (2012) 659.
22. A. Abouimrane, O. Compton, K. Amine and S. Nguyen, *J Phys Chem C*, 114 (2010) 12800.
23. T. Zheng, J. Xue and J. Dahn, *Chemistry of Materials*, 8 (1996) 389.
24. M. Liang and L. Zhi, *Journal of Materials Chemistry*, 19 (2009) 5871.
25. X. Yang, J. Zhu, L. Qiu and D. Li, *Adv. Mater.*, 23 (2011) 2833.
26. G. Wang, X. Sun, F. Lu, H. Sun, M. Yu, W. Jiang, C. Liu and J. Lian, *Small*, 8 (2012) 452.
27. F. Liu, S. Song, D. Xue and H. Zhang, *Adv. Mater.*, 24 (2012) 1089.
28. J. Kim, L. Cote and J. Huang, *Accounts of Chemical Research*, 45 (2012) 1356.
29. P. Touzain, R. Yazami and J. Maire, *Journal of Power Sources*, 14 (1985) 99.
30. M. Kim, D. Kim, Y. Kang and O. Park, *RSC Advances*, 5 (2015) 3299.
31. Z. Gao, W. Yang, J. Wang, N. Song and X. Li, *Nano Energy*, 13 (2015) 306.
32. E. Yoo, J. Kim, E. Hosono, H. Zhou, T. Kudo and I. Honma, *Nano Letters*, 8 (2008) 2277.
33. J. Mu, C. Hou, H. Wang, Y. Li, Q. Zhang and M. Zhu, *Science Advances*, 1 (2015) e1500533.
34. T. Hu, X. Sun, H. Sun, M. Yu, F. Lu, C. Liu and J. Lian, *Carbon*, 51 (2013) 322.
35. C. Wang, X. Wang, Y. Wang, J. Chen, H. Zhou and Y. Huang, *Nano Energy*, 11 (2015) 678.
36. S. Xiong, K. Xie, Y. Diao and X. Hong, *Journal of Power Sources*, 246 (2014) 840.
37. E. Markevich, G. Salitra and D. Aurbach, *ACS Energy Letters*, 2 (2017) 1337.

38. Y. Li, K. Leung and Y. Qi, *Accounts of Chemical Research*, 49 (2016) 2363.

© 2017 The Authors. Published by ESG (www.electrochemsci.org). This article is an open access article distributed under the terms and conditions of the Creative Commons Attribution license (<http://creativecommons.org/licenses/by/4.0/>).